QUARTERLY JOURNAL OF THE ROYAL METEOROLOGICAL SOCIETY
Q. J. R. Meteorol. Soc. **134**: 905–912 (2008)
Published online 6 June 2008 in Wiley InterScience
(www.interscience.wiley.com) DOI: 10.1002/qj.253

A climatological view of HNO_3 partitioning in cirrus clouds

M. Krämer,[a]* C. Schiller,[a] C. Voigt,[b] H. Schlager[b] and P. J. Popp[c,d]
[a] *Institut für Chemie und Dynamik der Geosphäre, Forschungszentrum Jülich, Germany*
[b] *Institut für Physik der Atmosphäre, DLR Oberpfaffenhofen, Germany*
[c] *NOAA Earth System Research Laboratory, Boulder, Colorado, USA*
[d] *Cooperative Institute for Research in the Environmental Sciences, University of Colorado, Boulder, USA*

ABSTRACT: A new *in situ* climatology of cirrus ice water content (IWC) is used, together with observed molar ratios of HNO_3/H_2O in cirrus ice particles, to estimate the range of HNO_3 content in cirrus ice in the temperature interval 185–240 K. We find that nearly over the complete temperature range HNO_3 percentages in ice between 0.01 and 100% are possible in cirrus clouds and that IWC is a major parameter determining the content of HNO_3 in ice at given temperatures. Considering average conditions, the HNO_3 content increases with decreasing temperature from 1% to about 10% in the range 240–200 K. For colder ice clouds, the average HNO_3 content again decreases down to 6%. At higher temperatures, less efficient HNO_3 uptake limits the HNO_3 content in cirrus ice, while at low temperatures small IWCs permit only little HNO_3 in ice, thus causing the convex-shaped average HNO_3 content curve. The highest HNO_3 content is expected in tropical ice clouds with very large IWCs, especially at temperatures between 190 and 210 K. Thus, tropical cirrus clouds show the highest potential to vertically redistribute HNO_3. Copyright © 2008 Royal Meteorological Society

KEY WORDS molar ratios; ice clouds; ice water content

Received 5 July 2007; Revised 14 March 2008; Accepted 25 March 2008

1. Introduction

Vertical redistribution of nitric acid (HNO_3) by sedimenting cirrus ice crystals is discussed as a possible mechanism for lowering upper tropospheric ozone. A reduction of the greenhouse gas ozone would give negative feedback to climate. The temperature in the tropopause region is very sensitive to changes in ozone mixing ratio. For example, Forster and Joshi (2005) estimate, based on a narrowband fixed dynamical heating model, that the annual average temperature change at the tropical cold-point tropopause for a 10% increase in ozone is 0.6 K. Meier and Hendricks (2002) report a maximum ozone reduction of about 14%, while recently von Kuhlmann and Lawrence (2006) estimated a lower maximum value of 5% by using a global-scale chemistry-transport model. However, the authors state that the largest uncertainty of this result is likely to be linked to the actual theory describing the HNO_3 uptake process on ice.

Dissociative Langmuir isotherms determining HNO_3 as equilibrium ice surface coverages have often been employed in models (e.g. by von Kuhlmann and Lawrence, 2006), but, as shown by Popp *et al*. (2004), could not satisfactorily fit atmospheric measurements. Kärcher (2005) and Krämer *et al*. (2006) show that adsorption of HNO_3 on the ice surfaces is not the only pathway for HNO_3 in ice, but that a substantial amount of HNO_3 may enter the ice via freezing of liquid ternary aerosol particles. Further, Kärcher (2005) demonstrates that another important pathway of HNO_3 in cirrus is trapping of HNO_3 by growing ice crystals.

Here, we derive parametrizations of the HNO_3 content in ice for use in global models from field measurements by using a new approch to describe the HNO_3 content of cirrus clouds for most atmospheric conditions.

The first step is to compile a large database of HNO_3 content in cirrus for a broad range of atmospheric conditions. In the last decade, several field campaigns were performed where the amount of HNO_3 in cirrus ice ($HNO_3{}^{ice}$) - amongst other parameters - was measured in different geographical regions (Table I).

Voigt *et al*. (2006) summarised average values of most $HNO_3{}^{ice}$ measurements and expressed them in terms of molar ratios $\mathcal{M}^{ice}_{HNO_3}$ by dividing $HNO_3{}^{ice}$ by the ice water content (IWC):

$$\mathcal{M}^{ice}_{HNO_3} = \frac{HNO_3{}^{ice}}{IWC}. \quad (1)$$

An increase of $\mathcal{M}^{ice}_{HNO_3}$ with decreasing temperature in the range 225–198 K and an increase of $\mathcal{M}^{ice}_{HNO_3}$ with increasing total HNO_3 (HNO_3^{total} = gas phase + particulate HNO_3) is found by Voigt *et al*. (2006).

Kärcher and Voigt (2006) expressed the same dataset as a fraction of HNO_3^{total} in ice

$$\mathcal{F}^{ice}_{HNO_3} = 100 \cdot \frac{HNO_3^{ice}}{HNO_3^{total}}, \quad (2)$$

* Correspondence to: M. Krämer, ICG-1, FZ Jülich, Germany.
E-mail: m.kraemer@fz-juelich.de

Table I. Projects measuring HNO_3 in cirrus ice.

SUCCESS 1996	Subsonic Aircraft: Contrail and Cloud Effects Special Study	Weinheimer *et al.* (1998)
POLSTAR 1998	Polar Stratospheric Aerosol Experiment	Schlager *et al.* (2000); Krämer *et al.* (2003)
INCA 2000	Interhemispheric differences in Cirrus properties from Anthropogenic emissions	Ziereis *et al.* (2004)
SOLVE–THESEO 2000	SAGE III Ozone Loss and Validation Experiment – Third European Stratospheric Experiment on Ozone	Kondo *et al.* (2003)
CRYSTAL–FACE 2002	Cirrus Regional Study of Tropical Anvils and Cirrus Layers – Florida Area Cirrus Experiment	Popp *et al.* (2004)
EUPLEX 2003	European Polar Stratospheric Cloud and Lee Wave Experiment	Voigt *et al.* (2006)
TROCCINOX 2005	Tropical Convection, Cirrus and Nitrogen Oxides Experiment	Voigt *et al.* (2007)
SCOUT–O_3 2005	Stratospheric–Climate Links with Emphasis on the Upper Troposphere and Lower Stratosphere	
CR–AVE 2005	Costa Rica – Aura Validation Experiment	Popp *et al.* (2007)

and proposed an increasing $\mathcal{F}^{\text{ice}}_{\text{HNO}_3}$ with decreasing temperature for 240–195 K. Combining Equations (1) and 2 yields

$$\mathcal{F}^{\text{ice}}_{\text{HNO}_3} = \mathcal{M}^{\text{ice}}_{\text{HNO}_3} \cdot 100 \cdot \frac{\text{IWC}}{\text{HNO}_3^{\text{total}}}. \qquad (3)$$

We here develop a climatology of average $\mathcal{F}^{\text{ice}}_{\text{HNO}_3}$ as well as the total range of HNO_3 content in cirrus ice in the temperature range 185–240 K. For that purpose, firstly the new *in situ* IWC climatology (Schiller *et al.*, 2008), derived from ten field campaigns and covering the temperature range 182–250 K, is used (see section 2.1). Secondly, a new climatology for $\mathcal{M}^{\text{ice}}_{\text{HNO}_3}$ is derived from the database of Voigt *et al.* (2006), extended by new observations down to temperatures of 185 K (section 2.2). The range of total available nitric acid $\text{HNO}_3^{\text{total}}$ is estimated based on observations, and the resulting $\mathcal{F}^{\text{ice}}_{\text{HNO}_3}$ climatology is presented in section 3.1.

Based on the newly derived climatological average of molar ratios $\mathcal{M}^{\text{ice}}_{\text{HNO}_3}$, the average content of HNO_3 in ice is presented for Arctic, midlatitude and tropical cirrus clouds in section 3.2. In section 3.3, the average vertical distribution of $\mathcal{F}^{\text{ice}}_{\text{HNO}_3}$ is shown.

2. IWC and $\mathcal{M}^{\text{ice}}_{\text{HNO}_3}$ climatologies

2.1. IWC of cirrus clouds

The IWC of cirrus clouds was observed during ten field experiments using the Lyman-α fluorescence Fast In situ Stratospheric Hygrometer (FISH; Schiller *et al.*, 2008) with a forward-facing inlet sampling total water (= gas phase + particulate water). IWC was determined as the difference between total water and water vapour saturation with respect to ice. From the comprehensive dataset representing 27 hours flight time inside 52 Arctic, midlatitude and tropical cirrus clouds, Schiller *et al.* (2008) derived a new *in situ* climatology of IWC for the temperature range 182–250 K (Figure 1). The climatology encompasses the range of observed IWC by means of temperature-dependent functions (given in Table II) for the maximum (green), mean (red, without convective events) and minimum (orange) IWC. Schiller *et al.* (2008) also provide functions for mean IWC including convective envents as well as median IWC. Here, the mean IWC is used because the properties derived from IWC depend on the ice volume (Equation (3)). The functions are derived as fits through values in 1 K temperature bins. Schiller *et al.* (2008) provide a detailed description of IWC observations, and the derivation of the climatology and uncertainties. However, it should be noted that the uncertainty of individual data points is 11–23% for the low IWC for 195–182 K and 8-11% for 250–195 K; hereby, a potential systematic error can be estimated by the accuracy of the FISH calibration of 6% (details in Schiller *et al.*, 2008). These uncertainties are small compared to the wide range of IWC observed for a particular temperature bin.

From Figure 1 it can be seen that the IWC decreases with decreasing temperature while covering several orders of magnitude for each temperature. The dataset underlying the climatology includes cirrus clouds at various stages of development – from just formed very thin cirrus via fully developed to almost dissipated cirrus. The strong variation of IWC at certain temperatures is caused by varying cooling of raising air parcels that form ice clouds. The stronger the cooling of a vertically moving air parcel, the higher is the IWC of the developing cirrus ice cloud. This is caused by the increasing difference in ice saturation at the temperature of the initial air parcel and the temperature after cooling. Consequently, the decrease of the IWC band with decreasing temperature reflects the exponential decrease of the ice saturation value.

Also plotted in Figure 1 are mean IWC observed during selected field campaigns (i.e. POLSTAR, TROCCINOX, SCOUT-O_3 and CR-AVE). These data points will be discussed individually in section 3.1.

2.2. Molar ratio $\mathcal{M}^{\text{ice}}_{\text{HNO}_3}$ in cirrus ice

HNO_3 in cirrus ice was measured in a series of field experiments by means of forward- and aft-facing inlets of total reactive nitrogen (NO_y) instruments, or mass spectrometers that measure HNO_3 specifically. For this

DOI: 10.1002/qj

work, we assume that condensed-phase reactive nitrogen measured by the NO_y instruments is HNO_3. The publications listed in Table I provide a description of the measurements and techniques. An intercomparison of the different methods measuring HNO_3 in ice is not yet available. Therefore, the uncertainty of $\mathcal{M}^{ice}_{HNO_3}$ is here estimated to be 20%, a range that covers possible differences between the methods.

Average values of the molar ratios $\mathcal{M}^{ice}_{HNO_3}$ are shown in Figure 2 for all experiments. (For better differentiation, the term 'average' is used in combination with HNO_3, while 'mean' is used for H_2O quantities, though both denotes the arithmetic mean value.) Most of the data points are taken from Voigt *et al*. (2006), reporting observations in the temperature range 195–240 K. Three new observations are added here, all representing averages of one cirrus penetration: one measurement is an extreme case of a very thin ice cloud, possibly in its formation stage (TROCCINOX 2005; Voigt *et al*., 2007) and two measurements are at very low temperatures (CR-AVE 2005 and SCOUT-O_3 2005). The latter measurements are especially important as they allow extension of the temperature range to less than 195 K, which is of particular importance for tropical cirrus.

$\mathcal{M}^{ice}_{HNO_3}$ generally increases with decreasing temperature, i.e. the concentration of HNO_3 in ice is higher at lower temperatures. Kärcher and Voigt (2006) attribute this behaviour to less efficient HNO_3 trapping at higher temperatures despite faster ice growth rates, caused by increasingly rapid escape of adsorbed HNO_3 into the gas phase. The broad range of $\mathcal{M}^{ice}_{HNO_3}$ at a certain temperature is caused by a varying amount of HNO_3^{total} and IWC, whereas increasing HNO_3^{total} or decreasing IWC raises $\mathcal{M}^{ice}_{HNO_3}$. As described for the IWC, the variation of $\mathcal{M}^{ice}_{HNO_3}$ at a certain temperature also reflects different stages in the lifetime of cirrus, and the varying stages of the uptake process at which equilibrium of HNO_3 with the ice surfaces is reached.

We here derive temperature-dependent functions for minimum, average and maximum $\mathcal{M}^{ice}_{HNO_3}$(Figure 2; Table II). The average function for $\mathcal{M}^{ice}_{HNO_3}$ is similar to that presented by Kärcher and Voigt (2006) by applying a trapping model for HNO_3 uptake into ice crystals (not shown here).

3. Partitioning of HNO_3 in cirrus clouds

3.1. Overall HNO_3 partitioning

We transform Equation (1) for ${HNO_3}^{ice}$

$$ {HNO_3}^{ice} = \mathcal{M}^{ice}_{HNO_3} \cdot IWC \tag{4} $$

and insert the climatology of IWC (Figure 1) and $\mathcal{M}^{ice}_{HNO_3}$ (Figure 2). The resulting potential range of the amount of HNO_3 taken up in cirrus clouds is displayed in Figure 3. The average curve (solid red) represents Equation(4) for the average $\mathcal{M}^{ice}_{HNO_3}$ (solid line in Figure 2) and the mean IWC (red line in Figure 1). The maximum (dashed green) and minimum (dotted orange) amounts of HNO_3 in ice are derived similarly.

On average, the potential of cirrus ice to take up HNO_3 is about 1–10 pptv over the whole temperature range, but the total span ranges from 0.005 pptv at low IWC or molar ratios $\mathcal{M}^{ice}_{HNO_3}$ up to about 35 ppbv in a situation where both IWC and $\mathcal{M}^{ice}_{HNO_3}$ are high.

The fractions of HNO_3^{total} taken up in cirrus ice ($\mathcal{F}^{ice}_{HNO_3}$) are derived from the IWC and $\mathcal{M}^{ice}_{HNO_3}$ functions under the assumption of minimum/average/maximum values of HNO_3^{total} = 0.02/0.1/0.8 ppbv by means of Equation (3) and are plotted in Figure 4. (The average of 0.1 ppbv corresponds to 2×10^{-8} hPa at 200 hPa given by Kärcher and Voigt (2006) as average over many field campaigns. The minimum/maximum values are chosen to describe a large range of atmospheric conditions. Smaller/larger HNO_3^{total} values are possible in specific situations, but would not affect the result discussed here.) At a given temperature nearly every value of $\mathcal{F}^{ice}_{HNO_3}$ between about 0.01 and 100% is possible in cirrus clouds over almost the the total temperature range.

Table II. Temperature-dependent functions for ice water content, IWC, and molar ratio of HNO_3/H_2O, $\mathcal{M}^{ice}_{HNO_3}$.

Parameter	Unit	Temperature (K)	Function exponent, E	Coefficients		
				a_0	a_1	a_2
IWC_{min}	(ppmv)	185–240	$(a_0 \cdot a_1^T + a_2)$	−29.0184	0.992003	4.7907
$IWC^{noconvec}_{mean}$	(ppmv)	185–240	$(a_0 \cdot a_1^T + a_2)$	−1190.68	0.967686	2.15584
IWC_{max}	(ppmv)	185–240	$(a_0 \cdot a_1^T + a_2)$	-4.72212×10^{18}	0.793983	2.5333
$IWC_{mean,arctic}$	(ppmv)	197–240	$(a_0 \cdot a_1^T + a_2)$	−8025.80	0.960043	2.5669
$IWC_{mean,midlat}$	(ppmv)	203–240	$(a_0 + a_1^T)$	−2.48507	0.0166517	–
$IWC^{noconvec}_{mean,tropics}$	(ppmv)	185–240	$(a_0 \cdot a_1^T + a_2)$	−21161.4	0.952294	1.82953
$\mathcal{M}^{ice}_{HNO_3 min}$	–	185–240	$\{-(a_0 \cdot a_1^T + a_2) - 1.1\}$			
$\mathcal{M}^{ice}_{HNO_3 avg}$	–	185–240	$\{-(a_0 \cdot a_1^T + a_2)\}$	−26.4641	1.00155	−30.6534
$\mathcal{M}^{ice}_{HNO_3 max}$	–	185–240	$\{-(a_0 \cdot a_1^T + a_2) + 1.3\}$			

IWC from Schiller *et al*., 2008; Functions are 10^E; noconvec = convective events are excluded from the climatology.

DOI: 10.1002/qj

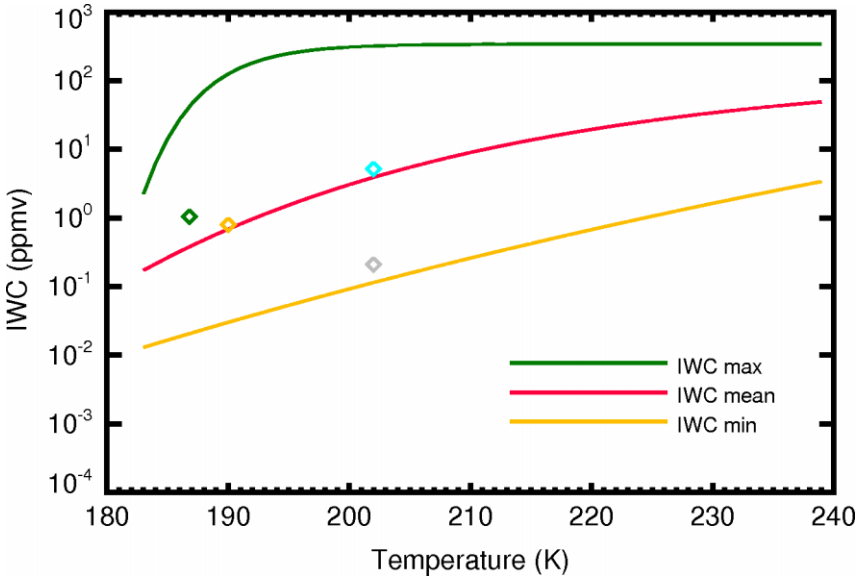

Figure 1. *In situ* climatology of maximum, mean (without convective events) and minimum ice water content (Schiller *et al*., 2008). Diamonds denote mean field observations; for colour code see Figure 2. This figure is available in colour online at www.interscience.wiley.com/qj

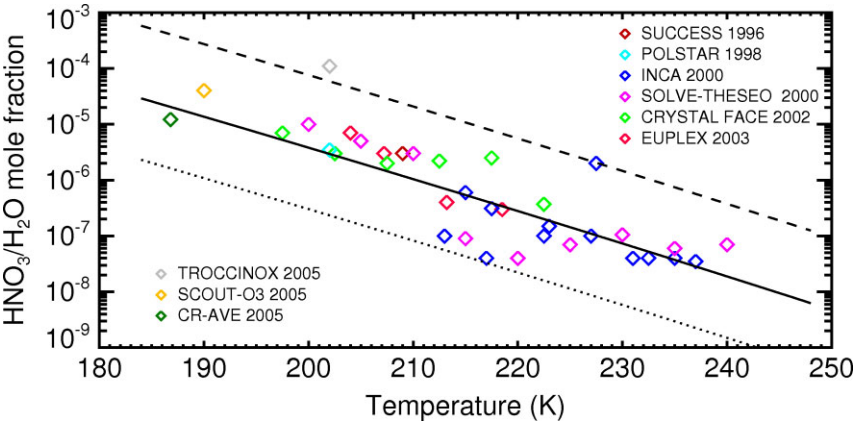

Figure 2. Molar ratio ($\mathcal{M}^{\mathrm{ice}}_{\mathrm{HNO_3}}$) of $HNO_3{}^{ice}$ to IWC in cirrus ice. Lines show maximum, average, and minimum molar ratios, diamonds are average field observations, and data points except SCOUT-O_3 and CR-AVE are adapted from Voigt *et al*. (2006, 2007). This figure is available in colour online at www.interscience.wiley.com/qj

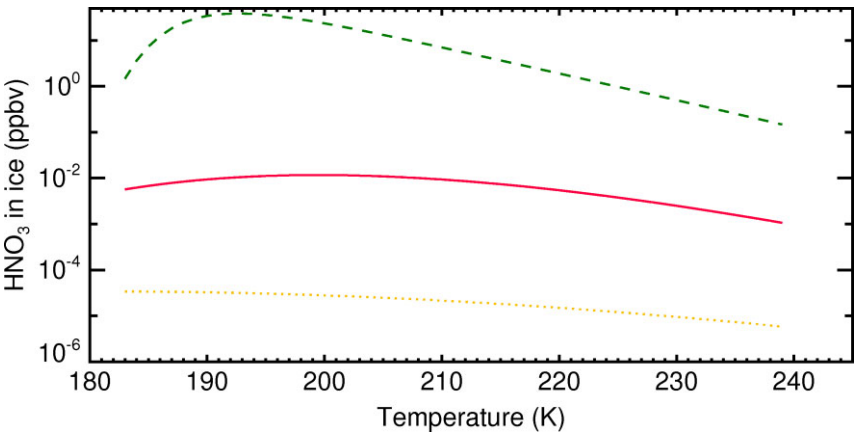

Figure 3. Maximum, average and minimum potential of HNO_3 uptake in cirrus ice. $HNO_3{}^{ice}$ is derived from Equation (1). This figure is available in colour online at www.interscience.wiley.com/qj

DOI: 10.1002/qj

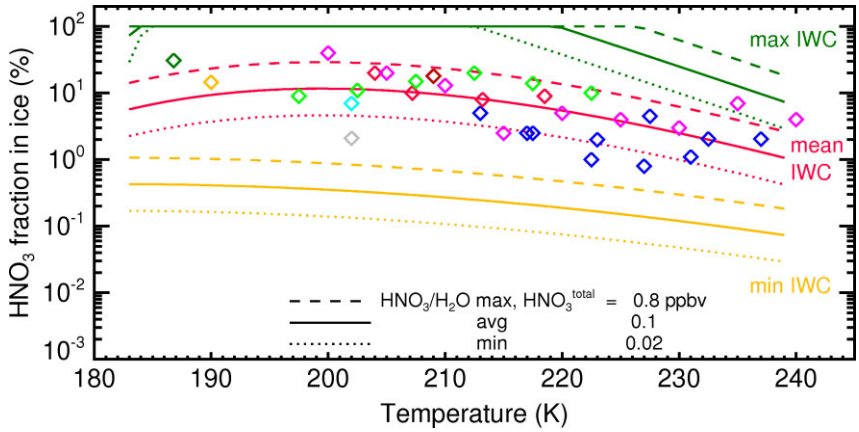

Figure 4. Fraction of HNO_3^{total} in cirrus ice ($\mathcal{F}^{ice}_{HNO_3}$), derived from Equation (3); minimum (dotted), average (solid) and maximum (dashed) for IWC minimum (orange), mean (red) and maximum (green). The respective HNO_3^{total} are indicated in the legend. Diamonds are average field observations; data points except TROCCINOX, SCOUT-O_3 and CR-AVE 2005 are from Kärcher and Voigt (2006). For colour code see Figure 2. This figure is available in colour online at www.interscience.wiley.com/qj

Figure 4 illuminates the mechanisms leading to this wide spread of $\mathcal{F}^{ice}_{HNO_3}$. The solid red line represents the average $\mathcal{F}^{ice}_{HNO_3}$ in cirrus ice (derived from mean IWC, average $\mathcal{M}^{ice}_{HNO_3}$ and average HNO_3^{total}). $\mathcal{F}^{ice}_{HNO_3}$ shows a slight convex form, increasing from about 1% to 10% when the temperature decreases from 240 K to about 200 K. For temperatures lower than 200 K, $\mathcal{F}^{ice}_{HNO_3}$ drops again to 6% at 185 K. The dotted (dashed) red curves encompassing the average $\mathcal{F}^{ice}_{HNO_3}$ represent mean IWC by using minimum (maximum) $\mathcal{M}^{ice}_{HNO_3}$ and minimum (maximum) HNO_3^{total}. Note here that the $\mathcal{F}^{ice}_{HNO_3}$ curves vary by only ± 0.05–5% when assuming the IWC and $\mathcal{M}^{ice}_{HNO_3}$ uncertainties shown in sections 2.1 and 2.2. An important result is that the large scatter in $\mathcal{M}^{ice}_{HNO_3}$ (Figure 2) and HNO_3^{total} causes a variation of only several percent in $\mathcal{F}^{ice}_{HNO_3}$.

The largest scatter in $\mathcal{F}^{ice}_{HNO_3}$ is caused by IWC. The orange curves represent the low range of 0.03 to 1% $\mathcal{F}^{ice}_{HNO_3}$ of thin cirrus clouds while the green curves represent cirrus clouds with a very high ice water mass; due to the high IWC, these clouds have the highest potential to efficiently scavenge the available HNO_3. For temperatures larger than 220 K, the maximum IWC is nearly constant (Figure 1), but $\mathcal{M}^{ice}_{HNO_3}$ is so small (Figure 2) that the HNO_3 could not be completely scavenged by the ice. Nevertheless, even here 4–100% HNO_3 could be taken up by cirrus. At 220–200 K, the steadily high maximum IWC, in combination with increasing $\mathcal{M}^{ice}_{HNO_3}$, results in a complete uptake of HNO_3 in cirrus ice at maximum IWC. In the range 200–185 K, the maximum IWC strongly decreases but, combined with the continuously increasing $\mathcal{M}^{ice}_{HNO_3}$, all available HNO_3 could still be scavenged by the ice. Below 185 K, the maximum IWC becomes so small that $\mathcal{F}^{ice}_{HNO_3}$ drops again despite the increasing $\mathcal{M}^{ice}_{HNO_3}$.

Obviously, IWC is the parameter mainly determining the content of HNO_3 in cirrus clouds at given temperatures. Thin cirrus clouds are not able to efficiently scavenge HNO_3, while thick cirrus can contain all available HNO_3. However, at higher temperatures the low $\mathcal{M}^{ice}_{HNO_3}$ molar ratio (caused by less efficient HNO_3 trapping; Kärcher and Voigt, 2006), and at low temperatures the low IWC, limits HNO_3 uptake in cirrus ice, thus causing the convex-shaped broad range describing the fraction of HNO_3 in cirrus ice clouds.

Also plotted in Figure 4 are observed average percentages of HNO_3^{total} in ice, $\mathcal{F}^{ice}_{HNO_3}$, from the field campaigns shown in Figure 2. (The data points represent different kinds of averages: INCA, SOLVE-THESEO, CRYSTAL FACE, EUPLEX have averages over temperature intervals, whereas SUCCESS, POLSTAR, TROCCINOX, SCOUT-O_3, CR-AVE have averages over single events; data points, except TROCCINOX, SCOUT-O_3 and CR-AVE 2005, are taken from Kärcher and Voigt, 2006.) Most of the data points group well around the presented average range of $\mathcal{F}^{ice}_{HNO_3}$. A closer look at some of the data lying outside (CR-AVE 2005, TROCCINOX 2005) shows that the high $\mathcal{F}^{ice}_{HNO_3}$ of CR-AVE 2005 could be caused by an IWC higher than the mean value (Figure 1). The low $\mathcal{F}^{ice}_{HNO_3}$ of TROCCINOX 2005 stems from the very low corresponding IWC. Data points showing typical IWCs and $\mathcal{M}^{ice}_{HNO_3}$, like POLSTAR 1998 and SCOUT-O_3 2005, are very close to the average $\mathcal{F}^{ice}_{HNO_3}$ curve.

Kärcher and Voigt (2006) derived the dependence on temperature of the average fraction of HNO_3 ($\mathcal{F}^{ice}_{HNO_3,avg}$) by applying a trapping model for HNO_3 uptake into ice crystals. Figure 5(b) shows a comparison of the modelled and our climatologically derived curve. Very good agreement between the model result and the climatology is seen in the temperature range 210–240 K. However, at lower temperatures, the simulated $\mathcal{F}^{ice}_{HNO_3,avg}$ steadily increases with decreasing temperature, while $\mathcal{F}^{ice}_{HNO_3,avg}$ from the climatology reported here shows the slight convex form discussed above.

This difference can be traced back to the climatology of IWC. The IWC used by Kärcher and Voigt (2006) is provided by Wang and Sassen (2002) from remote-sensing

DOI: 10.1002/qj

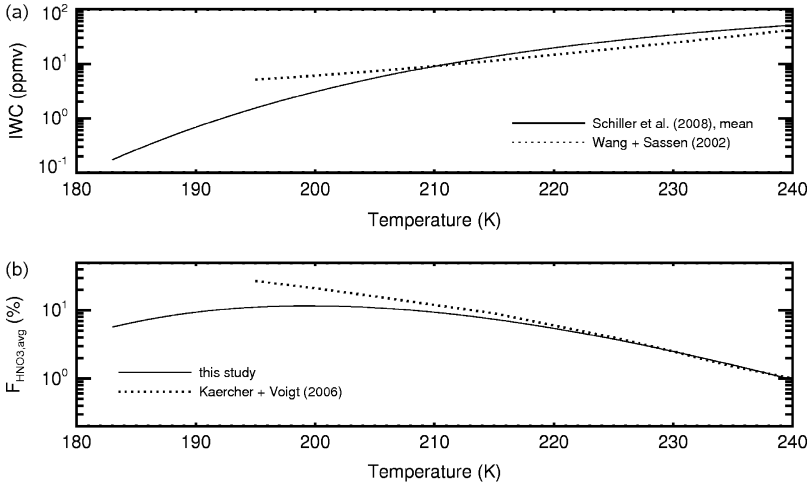

Figure 5. Comparison of (a) IWC climatologies (solid line is the mean used in this study, and dotted line is from Wang and Sassen, 2002), and (b) average fractions of total HNO_3 in cirrus ice (solid line is $\mathcal{F}^{\text{ice}}_{\text{HNO}_3,\text{avg}}$ of this study, and dotted line from Kärcher and Voigt, 2006).

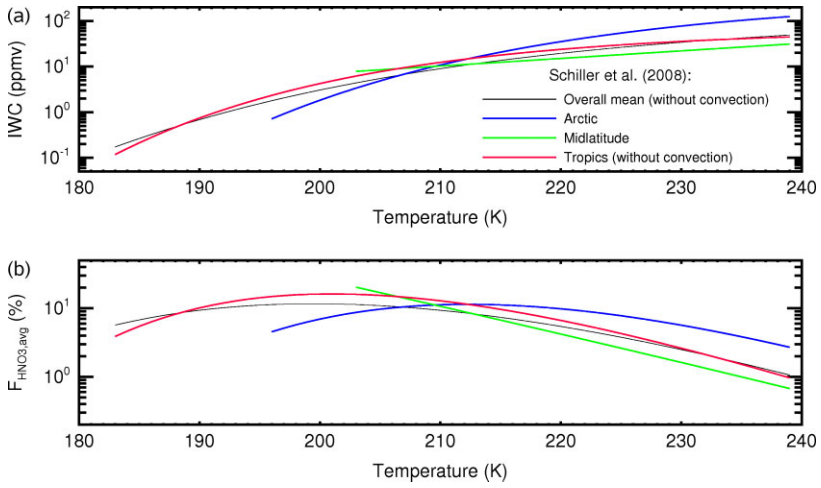

Figure 6. (a) Mean IWC functions provided by Schiller *et al.* (2008) and (b) average fractions of HNO_3^{total} in Arctic, midlatitude and tropical cirrus, derived from (a). This figure is available in colour online at www.interscience.wiley.com/qj

observations in midlatitude clouds in the temperature range 203–240 K and extrapolated down to 195 K by Kärcher and Voigt (2006) (Figure 5(a), dotted line). Compared to the IWC used here (Figure 5(a), solid line), the Wang and Sassen (2002) IWC is very similar for temperatures higher than about 210 K, but for lower temperatures (i.e. the extrapolated range) the IWC of the new *in situ* climatology (Schiller *et al.*, 2008) strongly decreases. A higher IWC leads to the higher HNO_3 fractions in ice with decreasing temperature reported by Kärcher and Voigt (2006), compared with the convex-shaped $\mathcal{F}^{\text{ice}}_{\text{HNO}_3}$ curve presented here.

3.2. Average HNO_3 in Arctic, midlatitude and tropical cirrus

Based on climatologies of mean IWC for Arctic, midlatitude and tropical cirrus (Figure 6(a); Schiller *et al.*, 2008), we derived the average HNO_3 fraction in ice, $\mathcal{F}^{\text{ice}}_{\text{HNO}_3,\text{avg}}$ (Figure 6(b)), from IWC together with average $\mathcal{M}^{\text{ice}}_{\text{HNO}_3}$ and HNO_3^{total} as described in the previous section.

Arctic cirrus (blue line). The temperature of Arctic cirrus is found to range between 196 and 240 K. $\mathcal{F}^{\text{ice}}_{\text{HNO}_3,\text{avg}}$ shows a convex shape similar to the overall average discussed in the previous section and here plotted for comparison (black line). The derivations of the Arctic mean IWC from the overall mean propagates to $\mathcal{F}^{\text{ice}}_{\text{HNO}_3,\text{avg}}$. The maximum $\mathcal{F}^{\text{ice}}_{\text{HNO}_3,\text{avg}}$ of 10% is found between 210 and 215 K, with smaller values at lower and higher temperatures.

Midlatitude cirrus (green line) are observed in the temperature range 203–240 K. The decrease of the mean IWC with temperature is low in midlatitude cirrus and does not show a convex shape. Thus, $\mathcal{M}^{\text{ice}}_{\text{HNO}_3}$ determines $\mathcal{F}^{\text{ice}}_{\text{HNO}_3,\text{avg}}$, resulting in a strong increase of HNO_3 fractional uptake in ice with decreasing temperature that reaches 20% at the lowest midlatitude cirrus temperature of 203 K. The temperature dependence of the midlatitude $\mathcal{F}^{\text{ice}}_{\text{HNO}_3,\text{avg}}$ is of the type proposed by Kärcher and Voigt (2006) (Figure 5(b), dotted curve).

Tropical cirrus (red line) cover the broadest temperature (185–240 K) and IWC range. $\mathcal{F}^{\text{ice}}_{\text{HNO}_3,\text{avg}}$ shows a

DOI: 10.1002/qj

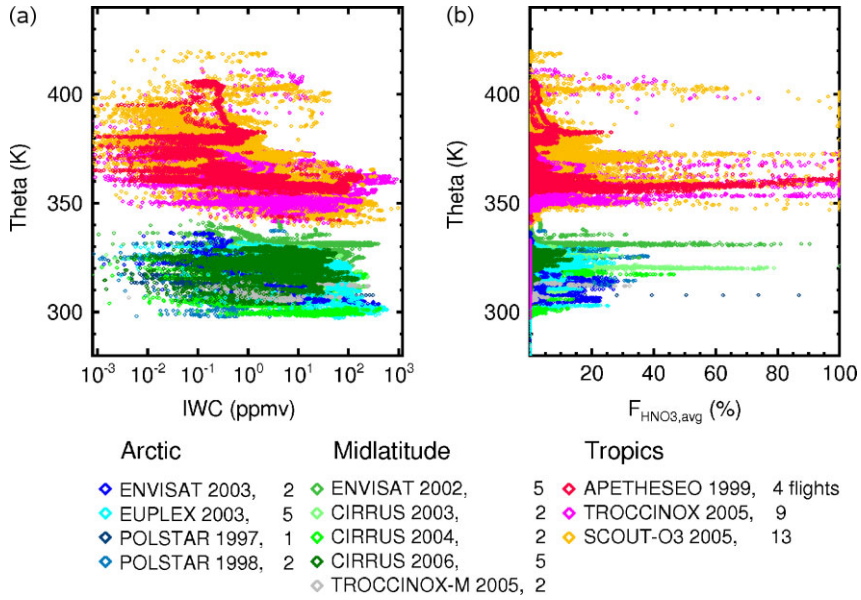

Figure 7. Potential temperature θ versus (a) IWC and (b) calculated average percentage HNO_3 uptake ($\mathcal{F}^{ice}_{HNO_3,avg}$) from 52 observed cirrus events, corresponding to 27 hours inside clouds. Bluish colours represent Arctic, greenish midlatitude and reddish tropical cirrus clouds. Schiller *et al*. (2008) gives details of the campaigns. This figure is available in colour online at www.interscience.wiley.com/qj

strong curvature, caused by the mechanisms explained in the previous section.

Apart from the varying temperature ranges, the differences in the mean IWC climatologies and HNO_3 partitioning in cirrus between the different geographical regions are moderate. Thus, we recommend considering the Arctic, midlatitude or tropical temperature ranges when using the climatologies for model simulations.

3.3. Vertical distribution of HNO_3 in cirrus

In section 3.1 we have shown that IWC mainly determines the HNO_3 content of cirrus clouds at a given temperature. Thus, we use the average function for $\mathcal{M}^{ice}_{HNO_3}$ (Table II) and the average HNO_3^{total} to convert single IWC data points taken at 1 Hz in Arctic, midlatitude and tropical field experiments to average HNO_3 fractions $\mathcal{F}^{ice}_{HNO_3,avg}$. The IWC data points are plotted in Figure 7(a) versus potential temperature θ. Note that the actual HNO_3 fraction data points may scatter only a little around the average as shown in Figure 4 since the influence of changes in HNO_3^{total} and $\mathcal{M}^{ice}_{HNO_3}$ is small compared to the influence of varying IWC. In Figure 7(b) the resulting $\mathcal{F}^{ice}_{HNO_3,avg}$ from 52 observed cirrus events, corresponding to 27 hours inside clouds, are plotted versus θ.

As shown in Figure 7(a), the upper IWC envelope of Arctic and midlatitude cirrus reaches values up to a few hundreds of ppmv H_2O throughout the observed θ range of 300–340 K. The tropical cirrus, found at higher θ levels, show a pronounced vertical structure: between 340 and 360 K, IWC reaches its maximum values of up to 1000 ppmv of condensed H_2O, then decreases to about 1 ppmv at about 380 K, where the tropical tropopause is located. The highest IWCs at θ 340–360 K, i.e. higher then 100–10 ppmv, are identified as deep convection events (Schiller *et al*., 2008). Likewise, the high IWCs detected above 380 K are attributed to overshooting events of deep convection. Here, IWC up to about 50 ppmv H_2O are found to be transported from the troposphere to the top of the tropical tropopause layer at 410–420 K.

The corresponding $\mathcal{F}^{ice}_{HNO_3,avg}$ (Figure 7(b)) show that in Arctic and midlatitude cirrus the upper envelope of HNO_3 content in ice increases from about 20% at 300 K to about 80% at 330 K. Tropical cirrus have the potential to take up all available HNO_3 between 350 and 370 K. Farther up at 380 K, where the cold-point tropopause is located, the maximum reaches only about 10%. In overshooting events above the tropopause, again high uptake of HNO_3 in cirrus up to 100% can be expected.

In summary, tropical cirrus clouds show the highest potential to vertically redistribute HNO_3. However, midlatitude cirrus at lower altitudes can also transport substantial amounts of HNO_3. Thus, below the tropopause a downward transport of HNO_3 by large ice crystals can occur. In addition, HNO_3 can be transported to the top of the tropical tropopause layer by overshooting deep convection events.

4. Summary and conclusions

We have provided a climatological view of the partitioning of HNO_3 in cirrus clouds in dependence on temperature. The analysis is based on a new *in situ* climatology of cirrus clouds IWC (Schiller *et al*., 2008), and a survey of molar ratios of HNO_3/H_2O in ice crystals, $\mathcal{M}^{ice}_{HNO_3}$. The major results are:

- The dataset of observed $\mathcal{M}^{ice}_{HNO_3}$(Voigt *et al*., 2006) is extended by new observations down to temperatures of 185 K and covers now the temperature range 185–240 K.

DOI: 10.1002/qj

- Functional relations for the temperature dependence of $\mathcal{M}^{\text{ice}}_{\text{HNO}_3}$ and the HNO_3 percentages in cirrus ice, $\mathcal{F}^{\text{ice}}_{\text{HNO}_3}$, are provided for the temperature range 185–240 K. In addition, regional averages of HNO_3 content in cirrus are provided for Arctic, midlatitude and tropical cirrus clouds (Table II; Equation (3)). These functions can be used in global climate models to constrain the impact of the HNO_3 content of ice particles on the upper tropospheric concentrations of ozone.
- From the HNO_3 climatology, IWC is identified as an important parameter determining the HNO_3 content in ice at given temperatures. The highest HNO_3 content of up to 100% is expected in thick tropical cirrus clouds, while very thin ice clouds carry maximally only 1% of the HNO_3.

  The average HNO_3 content in ice versus temperature is convex shaped: a maximum of about 10% HNO_3 is found in the range 200–210 K, and at higher and lower temperatures the HNO_3 content is smaller. At higher temperatures, low $\mathcal{M}^{\text{ice}}_{\text{HNO}_3}$ causes this decrease, while at lower temperatures the strong decrease of IWC is responsible for the low HNO_3 content in ice.

  The overall range of HNO_3 percentages in cirrus ice is estimated to 0.01 and 100% at given temperatures over nearly the whole temperature range. This reflects the variability of atmospheric conditions determining the HNO_3 content, which are cloud age and corresponding IWC, total available HNO_3, and the stage of the HNO_3 uptake process in relation to equilibrium.
- An average vertical distribution of the HNO_3 content of ice clouds is derived, showing that tropical convective cirrus clouds have, due to their high IWC, the highest potential to vertically redistribute HNO_3 by sedimenting ice crystals. Equally, HNO_3 may be uplifted by ice crystals to the top of the tropical tropopause layer in overshooting deep convection events.

The extent to which the upper tropospheric (and maybe lower stratospheric) chemistry can be disturbed by transport of HNO_3 through the tropical tropopause layer is an important issue for future investigations.

Acknowledgements

The authors thank the coordinators and all teams contributing to the field experiments compiled in the study presented here. Progress in the challenging task of providing an estimate of the nitric acid content of ice for most atmospheric conditions is only possible due to the large effort flowing into all the experiments.

Funding from various agencies for the different projects is acknowledged, in particular for SCOUT-O_3 which is funded by the EC within FP6 under contract GOCE-CT-2004-505390. C. Voigt appreciates funding by the Helmholtz Young Investigators Fund and the SFB-641 TROP-ICE. The authors also would like to thank Bernd Kärcher for stimulating discussions. As always, Rolf P. Müller is gratefully acknowledged.

References

Forster PMDF, Joshi M. 2005. The role of halocarbons in the climate change of the troposphere and stratosphere. *Climatic Change* **71**: 249–266.

Kärcher B. 2005. Supersaturation, dehydration, and denitrification in Arctic cirrus. *Atmos. Chem. Phys.* **5**: 1757–1772.

Kärcher B, Voigt C. 2006. Formation of nitric acid/water ice particles in cirrus clouds. *Geophys. Res. Lett.* **33**: L08806. DOI: 10.1029/2006GL025927.

Kondo Y, Toon OB, Irie H, Gamblin B, Koike M, Takegawa N, Tolbert MA, Hudson PK, Viggiano AA, Avallone LM, Hallar AG, Anderson BE, Sachse GW, Vay SA, Hunton DE, Ballenthin JO, Miller TM. 2003. Uptake of reactive nitrogen on cirrus cloud particles in the upper troposphere and lowermost stratosphere. *Geophys. Res. Lett.* **30**(4): 1154. DOI: 10.1029/2002GL016539.

Krämer M, Beuermann J, Schiller C, Grimm F, Arnold F, Peter T, Meilinger S, Meier A, Hendricks J, Petzold A, Schlager H. 2003. Nitric acid partitioning in cirrus clouds: a synopsis based on field, laboratory and model studies. *Atmos. Chem. Phys. Discuss.* **3**: 413–443.

Krämer M, Schiller C, Ziereis H, Bunz H. 2006. Nitric acid partitioning in cirrus clouds: the role of aerosol particles and relative humidity. *Tellus* **58B**: 141–147.

Meier A, Hendricks J. 2002. Model studies on the sensitivity of upper tropospheric chemistry to heterogeneous uptake of HNO_3 on cirrus ice particles. *J. Geophys. Res.* **107**: 4696. DOI: 10.1029/2001JD000735.

Popp PJ, Gao RS, Marcy TP, Fahey DW, Hudson PK, Thompson TL, Krcher B, Ridley BA, Weinheimer AJ, Knapp DJ, Montzka DD, Baumgardner D, Garrett TJ, Weinstock EM, Smith JB, Sayres DS, Pittman JV, Dhaniyala S, Bui TP, Mahoney MJ. 2004. Nitric acid uptake on subtropical cirrus cloud particles. *J. Geophys. Res.* **109**: D06302. DOI: 10.1029/2003JD004255.

Popp PJ, Marcy TP, Watts LA, Gao RS, Fahey DW, Weinstock EM, Smith JB, Herman RL, Troy RF, Webster CR, Christensen LE, Baumgardner DG, Voigt C, Karcher B, Wilson JC, Mahoney MJ, Jensen EJ, Bui TP. 2007. Condensed-phase nitric acid in a tropical subvisible cirrus cloud. *Geophys. Res. Lett.* **34**: L24812. DOI: 10.1029/2007GL031832.

Schiller C, Krämer M, Afchine A, Spelten N. 2008. An *in situ* climatology of ice water content in Arctic, midlatitude and Tropical cirrus. *J. Geophys. Res.* in press.

Schlager H, Petzold A, Ziereis H, Dörnbrack A, Grimm F, Arnold F, Schiller C. 2000. '*In situ* observations of particulate NOy in cirrus clouds for different atmospheric conditions'. Pp. 68–73 in *Proceedings of the European Workshop on Aviation, Aerosols, Contrails, and Cirrus Clouds, Seeheim, Germany*. Schumann U, Amanatidis GT (eds.) European Commission: Brussels.

Voigt C, Schlager H, Ziereis H, Kärcher B, Luo BP, Schiller C, Krämer M, Irie H, Kondo Y, Popp P. 2006. Nitric acid uptake in cirrus clouds. *Geophys. Res. Lett.* **33**: L05803. DOI: 10.1029/2005GL025159.

Voigt C, Kärcher B, Schlager H, Schiller C, Krämer M, de Reus M, Vössing H, Borrmann S, Mitev V. 2007. In-situ observations and modeling of nitric acid-containing particles in a cirrus cloud formation region. *Atmos. Chem. Phys.* **7**: 3373–3383.

von Kuhlmann R, Lawrence MG. 2006. The impact of ice uptake of nitric acid on atmospheric chemistry. *Atmos. Chem. Phys.* **6**: 225–235.

Wang Z, Sassen K. 2002. Cirrus cloud microphysical property retrieval using lidar and radar measurements. Part II: Midlatitude cirrus microphysical and radiative properties. *J. Atmos. Sci.* **59**: 2291–2303.

Weinheimer AJ, Campos TL, Walega JG, Grahek FE, Rodley BA, Twohy CH, Gandrud B. 1998. Uptake of NO_y on wave–cloud ice particles. *Geophys. Res. Lett.* **25**: 1725–1728.

Ziereis H, Minikin A, Schlager H, Gayet JF, Auriol F, Stock P, Baehr J, Petzold A, Schumann U, Weinheimer A, Ridle B, Ström J. 2004. Uptake of reactive nitrogen on cirrus cloud particles during INCA. *Geophys. Res. Lett.* **31**: L05115. DOI: 10.1029/2003GL018794.